Chapter 20
Concentrated Brine and Heat Dispersion into Shallow Coastal Waters of the Arabian Gulf

Sami Al-Sanea and Jamel Orfi

Abstract The main goal of this work is to assess the possible impacts of an existing desalination plant on the marine environment under various discharge conditions. Assessment is made through the determination, by using mathematical modeling, of the excess salinity and temperature distributions over the nominal seawater values as caused by the desalination plant effluent discharge. This chapter presents first a review of brine discharge models and studies followed by a rigorous numerical analysis study of a typical discharge problem into the Arabian Gulf. The mathematical formulation centers on the concept of shallow water equations in which the 3-D problem is reduced to an equivalent 2-D one by integrating the governing equations over the depth of flow. Appropriate boundary conditions, seabed friction, wind stress, and heat transfer correlations for thermal exchange at water-air interface are used. After validating the numerical model, it is applied to determine the salinity and temperature distributions in shallow coastal waters resulting from effluent discharge from an existing desalination plant situated on the Arabian Gulf. Parametric studies of the effects of a number of influential conditions are carried out by using the actual seabed topography and plant discharge and intake port locations. Effects of sea current magnitude and direction and plant discharge flow rate are in particular presented and analyzed. Possible plant discharge-intake port interactions were predicted with varying degrees of influence. The results presented indicated such interactions and quantified values of salinity and temperature at the plant intake port.

S. Al-Sanea (✉) · J. Orfi
Mechanical Engineering Department, King Saud University, Riyadh, Saudi Arabia
e-mail: sanea@KSU.EDU.SA

J. Orfi
e-mail: orfij@ksu.edu.sa

T.M. Missimer et al. (eds.), *Intakes and Outfalls for Seawater Reverse-Osmosis Desalination Facilities*, Environmental Science and Engineering,
DOI 10.1007/978-3-319-13203-7_20

20.1 Introduction

20.1.1 Background

The Kingdom of Saudi Arabia is undergoing rapid and massive development in all aspects including the industrial, power-generating, and desalination sectors. The existing desalination and power plants, in addition to those under construction and those planned for the future, need to be assessed with regard to their adverse impact on the natural environment, especially in shallow coastal regions. Analyzing existing and potential environmental problems and finding means to mitigate possible impacts are crucially important to the marine ecosystem as well as to the operating thermal efficiency of the desalination plants. Mathematical models provide an essential tool for predicting and analyzing impacts to help preclude possible design and implementation problems associated with outfalls.

Desalination plants consume huge amounts of energy to produce fresh water from seawater and return large quantities of warm, concentrated brine to the marine environment. The natural marine ecosystem may be adversely affected by possible increase in salinity and temperature, especially in shallow coastal regions.

In addition to the possible adverse impact a desalination plant discharge can have on the natural environment (particularly when discharged into shallow coastal waters), energy consumption and operating thermal efficiency of the plant can also be affected adversely. These problems are mainly related to:

- the energy needed for separating freshwater from seawater increases with increasing seawater salinity
- the fact that the efficiency of the plant cooling system deteriorates with increasing cooling water temperature.

The aforementioned problems may occur from possible recirculation of the heated and more concentrated brine effluents back into the intake port of the plant. In such a case, the plant would withdraw water from the sea at a salinity and temperature higher than the ambient seawater values. An increase in feed-water salinity from 4 to 5 %, for example, would require about 25 % more energy for seawater desalination.

It is therefore essential that the intake port of the desalination plant should withdraw seawater at the ambient salinity and temperature of the sea. Discharge-intake port interaction must, accordingly, be minimized. To achieve this, detailed information is required about the salinity and temperature distributions resulting from the plant discharge into the shallow coastal waters, and particularly in the vicinity of the plant. In addition, quite a few factors need to be considered and their corresponding effects be assessed through regulatory requirements and compliance. Such factors include: plant desalting capacity, plant site (coastline details and seabed topography), location of discharge and intake ports (separation distance and presence of natural or manmade barriers), sea-current speed and direction, and wind speed and direction.

20.1.2 Brine Discharge Models and Studies

Existing, operational desalination and power plants provide an indication of the types of environmental impact that need to be addressed. These impacts can be classified into several aspects such as liquid waste (concentrate), solid waste, gas emissions (CO_2), etc. The magnitude of impact from these sources of pollution will depend on the mode of desalination, or type of power generation plant, the type of fuel burned to generate the energy required for desalination, the geographical location of the facility, and the characteristics of the receiving waters.

Lattemann (2009) discussed the key concerns of desalination plant impacts on the marine environment in three regions, the Arabian Gulf, the Red Sea and the Mediterranean Sea. The author presented first an overview on the desalination capacities in these regions and focused on important factors affecting brine discharge problems such as intake and outfall structures and reject streams. The author described bio-fouling, scaling and corrosion and discussed methods for their respective control.

Bleninger and Jirka (2010) reviewed environmental impacts that can result from brine discharges. They reported results from available monitoring and laboratory studies and noted that the majority of studies focused on a limited number of species over a short period of time with no baseline data. The need for a more uniform assessment and monitoring approach was underlined. The socio-economic aspects related to brine discharge problems in several regions were also reviewed. The authors presented environmental standards for temperature, salinity, and residual chemicals as well as regulations on mixing zones. The results show that brine flow rates discharged into the sea are a large percentage of the intake rate; generally up to 40 % (Reverse Osmosis, RO) and up to 90 % (Multi Stage Flash, MSF, including cooling water). The brine flow rate is 4–5 times higher for thermal desalination than for RO processes relative to the amount of produced fresh water.

Table 20.1 gives the effluent salinity and temperature for the main desalination processes. One can see that the brine discharged salinity in RO can be as high as 85 g/kg for sea water desalination while in thermal processes, the salinity of the rejected brine should not exceed a certain allowable design value set by the $CaSO_4$ (Calcium Sulfate) solubility. This is in order to limit the risk of corrosion and scaling of the components of the desalination plant.

In addition, the effluent contains additives such as chemicals used for bio-fouling control and anti-scalants as well as corrosion products. Several studies analyzed the chemical aspects of brine discharge and impacts on the marine environment [see for example Ahmed et al. (2000) and Danoun (2007)]. Al Mutaz (1991) and Abdul Azis, et al. (2000) discussed impact of effluents from Saudi desalination plants in Jeddah (Red Sea) and Al-Jubail (Arabian Gulf) desalination plants, respectively.

Desalination specific environmental impact assessment (EIA) procedures were proposed by Hoepner (1999), while Alameddine and El-Fadel (2007) adopted discharge assessment methodology consisting of six phases. Munoz and Fernandez-Alba (2008) presented a life-cycle assessment methodology and showed that

Table 20.1 Effluent salinity and temperature for RO, MSF, and MED processes (adapted from Lattemann et al. 2009)

Brine property	Process		
	Reverse osmosis (RO)	Multi stage flash (MSF)	Multiple effect distillation (MED)
Brine concentration	65–85 g/kg (SWRO)	60–70 g/kg (brine)	60–70 g/kg (brine)
		Ambient salinity (cooling water)	Ambient salinity (cooling water)
	1–25 g/kg (BWRO)	45–50 g/kg (combined)	50–60 g/kg (combined)
Brine temperature (above ambient temperature)	Close to ambient temperature	3–5 °C (brine)	5–25 °C (brine)
		8–12 °C (cooling water)	8–12 °C or more (cooling water)
		5–10 °C (combined)	10–20 °C (combined)

RO Reverse Osmosis, *MED* Multiple Effect Distillation, *MSF* Multi Stage Flash

reverse osmosis desalination could significantly reduce its environmental impact if, instead of seawater resources, brackish groundwater resources were used.

Methods for brine rejection can be divided into two classes depending on whether the desalination plants are inland (evaporation pond method) or coastal (surface water discharge method). Alameddine and El-Fadel (2007) compared the advantages and disadvantages of various brine disposal options and proposed design recommendations for brine discharge. Bleninger and Jirka (2010) and Bleninger (2006) discussed the "zero liquid discharge" (ZLD) method which has the potential to provide freshwater without any brine discharges and impacts on the marine environment.

A desalination process separates the feed saline water, which can be brackish water or seawater, into product water with low salinity and concentrated brine wastes. The energy input required for a separation process is a function of several parameters including the separation process itself, the salinity, and the temperature of the incoming saline water. The minimization of this required energy is very important since it reduces the cost of producing fresh water and decreases the generation of greenhouse gases as well as decreases the disposal of various pollution products into the sea or atmosphere.

Several studies developed general relations for the minimum work input required for desalination processes using the second law of thermodynamics (Sharqawy et al. 2011; AlZahrani 2013). These relations determine the minimum work input per unit mass of fresh water produced for various feed saline water and fresh water salinities.

For practical situations, the energy required for desalination is much higher than that computed for the reversible separation due to the irreversibility occurring in each component (i.e. pump, evaporation chamber, membrane, valve, etc.) of each desalination process (MSF, MED, RO, etc.). In fact, current desalination processes require large amounts of electrical energy to operate different types of pumps (high pressure pumps, pumps to transport liquid streams, etc.) for the RO process or to heat steam for the evaporation process in thermal desalination plants such as MED and MSF.

Table 20.2 Energy consumption and gain output ratio (GOR, kg of product per kg of required steam) for the main industrial sea water desalination processes (Zhao et al. 2011)

Process	Temperature of heating steam (°C)	Top Temp. (°C)	GOR, kg/kg	Energy consumption	
				Thermal energy kJ/kg	Power kWh/m^3
MSF	130	120	10–12	185–227	2.5–4
	100	90	7–9	252–328	2.5–4
	80	70	4–5	462–567	2.5–4
MED-TVC	150	70	12–15	151–189	1.2–1.8
	120	70	10–12	189–231	1.2–1.8
LT-MED	90	80	10–13	177–231	1.2–1.8
	80	70	8–10	235–294	1.2–1.8
	70	60	6–8	294–395	1.2–1.8
VC					8–16
RO with energy recovery					5–6
RO without energy recovery					7–8

RO Reverse Osmosis, *MED* Multiple Effect Distillation, *MSF* Multi Stage Flash, *TVC* Thermal vapor compression, *LT* Low temperature

Table 20.2 gives the gain output ratio (GOR, defined as ratio of mass flow rate of permeate to mass flow rate of required steam) and energy consumption for the main industrial desalination processes at different conditions (Zhao et al. 2011). It shows in particular the MED-TVC (Thermal Vapor Compression) offers a higher performance in terms of GOR and energy consumption than the other thermal processes. Besides, the energy consumption for RO with recovery device is the lowest one.

The physical phenomena that act on the brine discharged into surface water bodies, such as a coastal sea, include advection, diffusion, convection, and buoyancy. The discharge process can be divided into the near field region nearest to the outfall discharge before boundary interaction (controlled by the source/discharge characteristics), and the far field region, where ambient transport mechanisms including ambient diffusion and advection dominate (Kuipers and Vreugdenhil 1973; Spalding 1975). An intermediate field separating the near and far fields can also be considered.

Representative studies on brine and heat dispersion in receiving water bodies are reviewed here with emphasis on those most relevant to the present work. Among the classical and pioneering studies in which the mathematical modeling of free surface flows has been explained comprehensively are those of Kuipers and Vreugdenhil (1973), Spalding (1975) and Rodi (1978). Kuipers and Vreugdenhil (1973) presented a detailed account on the nature of shallow water flows and the derivation of the depth-averaged equations.

Al-Sanea (1982) developed a finite-volume numerical procedure for the calculation of two-dimensional depth-integrated shallow-water flows. The procedure was based on depth correction analogous to the pressure correction procedure on which

the very well-known SIMPLE algorithm of Patankar and Spalding (1972) was based; see also Patankar (1980). Subsequently, Al-Sanea (1993) developed a model based on the computer program 2/E/FIX of Pun and Spalding (1977) (Al-Sanea et al. 1980) for calculating the flow and salinity distribution resulting from desalination plant discharges into shallow waters. The model accounted for the physical features that affect the concentrated brine dispersion process including convective and diffusive transport, wind stresses, seabed friction, and variable seabed elevation. Results of a parametric study for a hypothetical desalination plant effluent discharge under a range of meteorological, hydrological, topographical, and plant operating conditions, demonstrated the importance of the various factors that act on brine dispersion. Salinity contours have shown possible scenarios in which plant discharge can affect intake under different conditions. Heat transfer was, however, not included in the model.

More recent studies include those of Purnama et al. (2003) who used an analytical model to solve the transient salinity diffusion-advection equation in order to investigate dispersion of brine waste discharges into sea. A sloping sandy beach was considered in which the seabed depth increased until reaching a constant depth. Contours of salt concentration were presented. Employing the same model, Purnama and Al-Barwani (2005) studied means to minimize shoreline salinity levels without building a longer sea outfall. Such means consisted of creating a jump discontinuity on a seabed depth profile as well as keeping outfall location in the deeper region. A similar analytical model was used by Shao et al. (2008) to study effects of oscillatory tidal currents on brine discharge characteristics into shallow coastal water with a flat seabed. Results presented showed increase of salinity in coastal waters in vicinity of outfall and along shoreline due to continuous brine discharges.

Purnama and Al-Barwani (2006) solved the 2-D advection-diffusion equation for salt concentration to investigate effect of a tidally oscillating flow in dispersing brine waste discharge into sea. The geometry was simplified by using a straight coast with a constant water depth. The diffusive process was represented by dispersion coefficients and the brine waste was discharged at a constant rate. The plume was assumed to be vertically well mixed over the water depth. Results showed that, due to flow oscillation, the plumes also spread towards the upstream side of the outfall. However, by simulating a longer outfall, the potential impact of brine discharges into the sea could be reduced.

Al-Barwani and Purnama (2007) studied the effect of beach erosion on dispersing the brine waste discharged into sea. The authors used the same model used in Prunama and Al-Barwani (2006) but under steady-state conditions and allowing the seabed depth to vary as a power function of distance from the beach and neglecting the dispersion term in the longitudinal direction along the beach. The study is relevant to a plant that is built and operated with an outfall to satisfy imposed site environmental regulation compliance but the beach is subsequently being eroded.

A number of studies have used the Cornel Mixing Zone Expert System CORMIX developed by Jirka and co-authors (Doneker and Jirka 2001). This tool combines a series of software systems for analysis, prediction, and design of aqueous discharges into watercourses. The system provides comprehensive

approach to mixing zone analysis, regulatory assessment, and outfall design (Donecker and Jirka 2001). The CORMIX methodology is based on the role of boundary interaction on mixing and uses several hydrodynamic criteria and physical concepts such as the length scale, jet to plume transition, jet to cross flow length scale concept.

Alameddine and El-Fadel (2007) used CORMIX to simulate dispersion of a brine plume in a marine environment by considering the discharge of heated effluent from a desalination-power plant into the Arabian Gulf. The authors compared the mixing behavior and efficiency of surface, submerged single-port, and submerged multi-port outfalls. Results revealed the inadequacy of using surface discharge outfalls for brine disposal. A multi-port discharge proved to be adequate to enhance dilution rates, whereby a tenfold dilution rate was achieved within a 300 m mixing zone. The authors highlighted several limitations of the CORMIX model including its limited capability for simulating the discharge of large flow volumes into shallow areas.

Malcangio and Petrillo (2010) used a 3-D model to simulate brine discharge from desalination plants into a coastal region in southern Italy characterized by presence of protected vegetation species. The Reynolds Averaged Navier-Stokes equations (RANS) were considered and data on topography of target area and climatic conditions were introduced in the model. Results in terms of excess salinity were analyzed and the most suitable location for the brine outfall was determined.

Palomar and Losada (2011) discussed three basic approaches for modeling impact of brine discharge on the marine environment. These are: (i) models based on a dimensional analysis of the phenomenon, (ii) models based on integration of differential equations along the cross section of flow, and (iii) hydrodynamic models. The first and second types of models are based on several assumptions and restrictions reducing in general their accuracy and reliability. The hydrodynamic models solve the conservation equations of mass, momentum, and constituents. The energy equation is not solved in general. Compared to the other types of models, the hydrodynamic models are more rigorous, capable of modeling coupled, complex phenomena, and simulation of different configurations of discharge, intake, and ambient conditions. However, these models present two major limitations; firstly, coupling between near field and far field is difficult due to different spatial and time scales and, secondly, long computational time is required.

Palomar et al. (2012) examined modeling of near field brine discharge and analyzed assumptions, capability, limitations, and reliability of steady-state models used. These models were either based on dimensional analysis such as CORMIX or based on integration of differential equations such as CORJET, VISUAL PLUMES, and VISJET. The authors noted that the lack of validation studies of negatively buoyant jets was a common shortcoming in these commercial models. Significant errors were detected in the sensitivity analyses carried out. Palomar et al. (2012) focused on the validation of these models via performing many tests simulating different cases and using available published experimental data. The authors outlined limitations of each tool and detected errors and discrepancies that could result in the underestimation of dilution by as much as 60–90 %.

A simple model for simulating behavior of dense jets was developed by Cipollina et al. (2004). Cipollina's model considered four basic jet parameters, namely, flow rate, density, inclination, and diameter. The velocity and concentration distributions around the jet axis were assumed to be Gaussian and the entrainment velocity was supposed to be proportional to local jet velocity. Results included information on trajectory, spreading, and dilution of inclined dense jets. Abou-Elhaggag et al. (2011) investigated jet trajectory and dilution of submerged negatively-buoyant jet discharging vertically over a flat bottom in a calm ambient environment. Experimental observations made for terminal height of rise of dense jets and for concentration profiles along jet trajectory were used to validate a numerical model by using the FLUENT package. Various port diameters and concentration of effluent salinities were investigated and a new model for the terminal height of rise of dense jets was proposed.

Fernadez et al. (2012) studied the accuracy of four mixing zone models by conducting a comparative study with brine discharge measurements from a reverse osmosis desalination plant in Spain. The authors concluded that each model was conservative in its results except one model whose predictions were very close to measured data. Very recently, Oliver et al. (2013) developed an integral model to predict the near field behavior of negatively buoyant discharges in quiescent ambient fluid. The model included influences of additional mixing associated with buoyancy induced instabilities. Comparisons were carried out with predictive models and experimental data.

20.1.3 Current Status and Objectives of Present Work

The previous section has reviewed studies and considered a number of important issues related to brine discharges from desalination/power plants. It is clear that there is a continuing need for assessment of environmental impact of brine discharges from desalination plants as well as assessment of likely flow interaction between plant discharge and intake ports. While the former assessment concerns environment protection, the latter assessment concerns thermal efficiency of the plant and the energy required for desalination. These assessments can only be made by knowledge of detailed temperature, chemical pollutants, and brine distributions in bodies of water resulting from plant effluent discharges. The main concluding remarks of this review can be summarized as follows:

- Bodies of water where concentrated brine and heat are discharged can broadly be classified as shallow waters and deep waters. For each class, different mathematical models apply with specific features.
- The problem of desalination plant discharge-intake port interaction has in large been overlooked despite its possible effect on increasing feed water salinity and hence a likely increase in energy required for salt separation as part of the desalination process.

- Reducing energy consumption for desalination is crucial. Efforts should focus to improve plant performance, minimize discharge-intake port interaction, and reduce environmental impact.
- Few studies have considered thermal analysis. Thus, the energy equation was typically not included in previous models of brine disposal from desalination plants.
- More emphasis was given to the near field analysis, while only a small number of studies investigated the far field. Coupling between near and far fields is important and Computational Fluid Dynamics (CFD) models are potentially capable for such coupling and analysis.
- The majority of brine and heat dispersion studies, particularly those based on analytical tools, have adopted simplified mathematical models with various limiting assumptions. Few studies have used rigorous mathematical models.

The purpose of this work is to present and validate a numerical model for predicting brine and heat dispersion into shallow coastal waters. The mathematical formulation centers on the concept of shallow water equations in which the 3-D problem is reduced to an equivalent 2-D one by integrating the governing equations over the depth of flow.

After validating the numerical model, it is applied after appropriate modifications to determine the salinity and temperature distributions in shallow coastal waters resulting from effluent discharge from an existing desalination/power plant situated on the Arabian Gulf. Parametric studies of the effects of a number of influential conditions are carried out by using the actual seabed topography and plant discharge and intake port locations. Brief information on all of these aspects as well as the discharged mass flow rate and variable water depth are given later. Next, the mathematical formulation and numerical solution procedure are presented.

20.2 Mathematical Formulation

20.2.1 Shallow Water Approximations

The final form of the mathematical model to be employed in the study is based on the shallow-water approximations. Therefore, the governing equations are depth-averaged (integrated) by assuming negligible variations of velocity and temperature over the depth and by neglecting the vertical velocity component, thus rendering the three-dimensional problem to be two-dimensional. Further, the eddy viscosity and diffusivity coefficients are assumed constant. These assumptions are in harmony with the free-surface-flow approximations in shallow and wide stretches of water (Kuipers and Vreugdenhil 1973; Spalding 1975; Al-Sanea 1982, 2010; Al-Sanea and Orfi 2013).

Figure 20.1 shows a schematic of the modeled flow domain. The flow is bounded below by a rigid, fixed surface $z = z_b$ (x, y) and by a free surface $z = z_b$ (x, y) + h (x, y, t) above a horizontal datum-plane and subjected to atmospheric

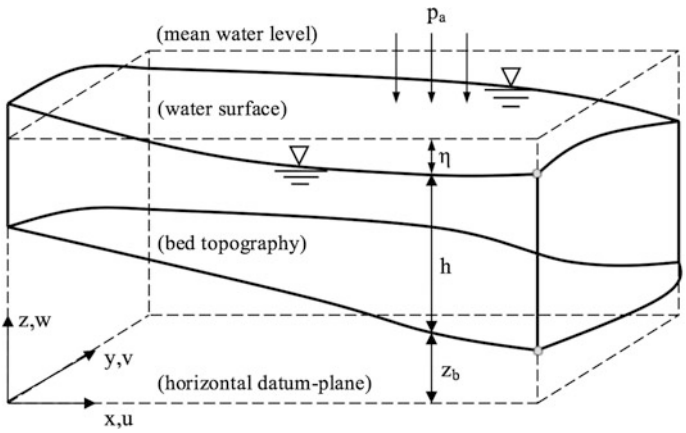

Fig. 20.1 Definition of bottom height, depth, mean water level, and water surface (Al-Sanea 1982)

pressure (p_a), where h is the local water depth. The integration is carried out from the bottom to the surface, i.e. from z_b to $z_b + h$. The depth-averaged quantities are defined by the following relations:

$$\bar{u} = \frac{1}{h}\int_{z_b}^{z_b+h} u\, dz, \quad \bar{v} = \frac{1}{h}\int_{z_b}^{z_b+h} v\, dz, \quad \text{and} \quad \bar{\tau} = \frac{1}{h}\int_{z_b}^{z_b+h} \tau\, dz \tag{20.1}$$

On integrating the equation system, making use of Leibnitz's rule and the kinematic boundary conditions at the surface and bottom (see Al-Sanea 1982 for details), one obtains the depth-averaged conservation equations.

20.2.2 The Governing Differential Equations Solved

20.2.2.1 Further Basic Assumptions

So far, the only approximations made to the three-dimensional Navier-Stokes equations, in deriving the general shallow-water equations, are:

1. The assumption of a hydrostatic pressure distribution.
2. The fluid is assumed to be incompressible and homogenous.
3. Gain or loss of mass from surface (rain, evaporation) and bottom (seepage) are not considered.
4. The vertical velocity profiles are approximated to be nearly uniform; hence depth-averaged values are used.
5. The wind and bottom stresses are related to the square of the depth-averaged velocities (Al-Sanea 1982).

6. The fluid stresses are expressed by a constant laminar- or eddy-viscosity coefficient multiplying the depth-averaged velocity gradients (Al-Sanea 1982).

In the present formulation, it is further assumed that (Spalding 1975):

7. The flow is steady.
8. The "rigid-lid" approximation is valid; however, the bed topography can vary.
9. Flow over small stretches of water; hence, negligible atmospheric-pressure variation.

20.2.2.2 The Resulting Governing Equations

Subject to the above assumptions the system of equations reduces to:

Conservation of mass

$$\frac{\partial}{\partial x}(h\,\bar{u}) + \frac{\partial}{\partial y}(h\,\bar{v}) = 0 \tag{20.2}$$

where $\bar{u}$ and $\bar{v}$ are the depth-averaged velocity components in the x- and y-directions, respectively, and h is the local depth of flow.

Conservation of u-momentum

$$\frac{\partial}{\partial x}(h\,\bar{u}^2) + \frac{\partial}{\partial y}(h\,\bar{u}\,\bar{v}) - \frac{1}{\rho}\frac{\partial}{\partial x}\left(h\,\bar{\mu}_{eff}\frac{\partial \bar{u}}{\partial x}\right) - \frac{1}{\rho}\frac{\partial}{\partial y}\left(h\,\bar{\mu}_{eff}\frac{\partial \bar{u}}{\partial y}\right) = S_u \tag{20.3a}$$

where ρ is the water density, $\bar{\mu}_{eff}$ is the effective viscosity and S_u is the source term for u and is given by:

$$S_u = -\frac{h}{\rho}\frac{\partial p}{\partial x} + h f\,\bar{v} - C_f \bar{u}(\bar{u}^2 + \bar{v}^2)^{1/2} + C_s\frac{\rho_{air}}{\rho}U_o(U_o^2 + V_o^2)^{1/2} \tag{20.3b}$$

where p is the static pressure, f is the Coriolis parameter, C_f is the seabed friction factor, C_s is the wind force friction factor, ρ_{air} is the air density, U_o and V_o are the wind relative velocities with respect to the water velocity in the x- and y-directions, respectively.

Conservation of v-momentum

$$\frac{\partial}{\partial x}(h\,\bar{u}\,\bar{v}) + \frac{\partial}{\partial y}(h\,\bar{v}^2) - \frac{1}{\rho}\frac{\partial}{\partial x}\left(h\,\bar{\mu}_{eff}\frac{\partial \bar{v}}{\partial x}\right) - \frac{1}{\rho}\frac{\partial}{\partial y}\left(h\,\bar{\mu}_{eff}\frac{\partial \bar{v}}{\partial y}\right) = S_v \tag{20.4a}$$

where S_v is the source term for v and is given by:

$$S_v = -\frac{h}{\rho}\frac{\partial p}{\partial y} - h f\ \bar{u} - C_f \bar{v}(\bar{u}^2 + \bar{v}^2)^{1/2} + C_s \frac{\rho_{air}}{\rho} V_o (U_o^2 + V_o^2)^{1/2} \qquad (20.4b)$$

Conservation of energy

$$\frac{\partial}{\partial x}(h\ \bar{u}\ \bar{T}) + \frac{\partial}{\partial y}(h\ \bar{v}\ \bar{T}) - \frac{1}{\rho}\frac{\partial}{\partial x}\left(h\ \frac{\bar{\mu}_{eff}}{\sigma_T}\frac{\partial \bar{T}}{\partial x}\right) - \frac{1}{\rho}\frac{\partial}{\partial y}\left(h\ \frac{\bar{\mu}_{eff}}{\sigma_T}\frac{\partial \bar{T}}{\partial y}\right) = \frac{S_T}{c_p} \qquad (20.5)$$

where $\bar{T}$ is the depth-averaged temperature, σ_T is the turbulent Prandtl number, c_p is the specific heat, and S_T is the source (or sink) term for T and represents energy interaction at the air-water interface. Convection heat transfer and evaporation effects may be accounted for in the energy equation through this S_T term.

Conservation of chemical species

$$\frac{\partial}{\partial x}(h\bar{u}\,\bar{c}) + \frac{\partial}{\partial y}(h\bar{v}\,\bar{c}) - \frac{1}{\rho}\frac{\partial}{\partial x}\left(h\frac{\bar{\mu}_{eff}}{\sigma_c}\frac{\partial \bar{c}}{\partial x}\right) - \frac{1}{\rho}\frac{\partial}{\partial y}\left(h\frac{\bar{\mu}_{eff}}{\sigma_c}\frac{\partial \bar{c}}{\partial y}\right) = S_c \qquad (20.6)$$

where $\bar{c}$ is the depth-averaged concentration of a chemical species in the solution, e.g. salt or salinity (Al-Sanea 1993), σ_c is the turbulent Schmidt number, and S_c is the source (or sink) term for c which is normally zero.

20.2.2.3 The Common Form of Transport Equation

All the above governing equations can be recast in the common form of a single general transport equation given below, enabling one solution procedure for all equations.

$$\frac{\partial}{\partial x}(h\bar{u}\,\bar{\phi}) + \frac{\partial}{\partial y}(h\bar{v}\,\bar{\phi}) - \frac{1}{\rho}\frac{\partial}{\partial x}\left(h\,\bar{\Gamma}_{eff,\phi}\frac{\partial \bar{\phi}}{\partial x}\right) - \frac{1}{\rho}\frac{\partial}{\partial y}\left(h\,\bar{\Gamma}_{eff,\phi}\frac{\partial \bar{\phi}}{\partial y}\right) = S_\phi \qquad (20.7)$$

where $\bar{\phi}$ is the general depth-averaged variable and stands for 1, $\bar{u}$, $\bar{v}$, $\bar{T}$, and $\bar{c}$ in Eqs. (20.2) through (20.6), respectively; $\bar{\Gamma}_{eff,\phi}$ is the effective exchange (diffusion) coefficient and stands for 0, $\bar{\mu}_{eff}$, $\bar{\mu}_{eff}$, $\bar{\mu}_{eff}/\sigma_T$, and $\bar{\mu}_{eff}/\sigma_c$ in Eqs. (20.2) through (20.6), respectively; and S_ϕ is the appropriate source and/or sink of the variable concerned ($\bar{\phi}$) which takes various expressions or be equal to zero.

20.2.2.4 Boundary Conditions

Solid Boundaries

The velocity components at solid boundaries are set to zero. The gradient of temperature and salinity in the direction normal to the solid boundaries is also set to zero.

Discharge Port

The velocity at the discharge port is fixed according to the discharge port area and the total mass flow rate of the effluent discharged to the sea. The temperature and salinity at the discharge port equal those of the heated and saline water coming out of the plant.

Intake Port

The velocity at the intake port is fixed according to the intake port area and the total mass flow rate withdrawn from the sea to the plant. However, the temperature and salinity at the intake port are unknown and calculated by the iterative solution procedure as an output from the computer model.

Sea Inlet and Sea Free Stream Boundaries

The velocity components are prescribed values as relevant to sea current with salinity and temperature values corresponding to ambient sea values. The sea current speed and direction are assumed nominal values and are also varied through a parametric study.

Sea Outlet Boundary

The velocity, salinity, and temperature gradients normal to this boundary are set to zero.

Thermal Interchange at Water-Air Interface

The heat rejected from the plant disperses into the sea water and is ultimately exchanged with the atmosphere from the water surface. Details of energy balance giving the net thermal interchange at the water-air interface are given in Spalding (1975), Al-Sanea (2010) and Al-Sanea and Orfi (2013). The equilibrium seawater

temperature is calculated in the absence of external thermal load, due to plant discharge, and used in the energy balance, see Al-Sanea and Orfi (2013).

Wind Stress and Seabed Friction

These are accounted for through appropriate correlations and introduced by the source terms in the momentum equations, see Eqs. (20.3b and 20.4b).

20.3 Numerical Solution Procedure and Model Validation

Due to space limitation, the numerical solution procedure and numerical model validation are briefly described in this section. More details can be found in Al-Sanea (2010) and Al-Sanea and Orfi (2013). It suffices to mention here that the stage of model validation is conducted prior to computer model application to a case study. The latter involves determining the salinity and temperature distributions in shallow coastal waters resulting from effluent discharge from an existing desalination plant situated on the Arabian Gulf.

20.3.1 Numerical Solution Procedure

The computer model used in this study is developed in-house by the first author and is an extension of that originally developed by Al-Sanea (1993) based on the 2/E/FIX CFD computer code of Pun and Spalding (1977) (Al-Sanea et al. 1980). The numerical solution procedure used employs the control-volume finite-difference method for the discretization of the depth-integrated conservation equations appropriate to shallow free-surface water flows. This computer code employs the well-known SIMPLE algorithm of Patankar and Spalding (1972) and Patankar (1980).

20.3.2 Numerical Model Validation

Numerical model validation was conducted in two stages which required appropriate model modifications. A preliminary stage was conducted by comparing numerical results with closed-form analytical solutions derived for 1-D channel flows with heat transfer. Results showed that the agreement between numerical model predictions and analytical results was excellent, see Al-Sanea and Orfi (2013) for details. The second stage of model validation considered a more

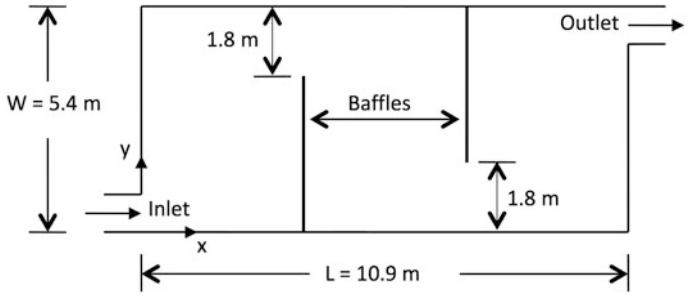

Fig. 20.2 *Top view* of the geometrical configuration of the experimental cooling pond of Cerco (1977) used to validate the present numerical model

challenging problem by comparing numerical results with 2-D flow and heat transfer in shallow cooling ponds in which temperature measurements were available under controlled laboratory conditions. Cerco (1977) used laboratory measurements to provide detailed data for the design of shallow experimental cooling ponds. He used various designs and baffle arrangements for the pond and evaluated performance for different flow rates.

Figure 20.2 describes a geometrical configuration of the experimental cooling pond used for validation of the present numerical model. Figure 20.3a through d presents dimensionless temperature profiles at the middle of the pond (X = 0.5) and across its width Y showing comparisons between present numerical predictions and experimental data of Cerco (1977) for four different cases. These cases involve different mass flow rates in the presence or absence of baffles. It is concluded that the agreement between predictions and measurements is, in general, quite good, see Al-Sanea and Orfi (2013) for details.

Besides, a grid independence study was conducted in which different sizes of the finite-volume grid were employed and their effects on the results were investigated accordingly. A grid of 40 × 33 (40 nodes in the x direction) was selected for use in all production runs.

20.4 Application to a Desalination Plant Discharge

After validating the mathematical model as briefly described in the previous section, the present section concerns model application to a case study. The case study involves the determination of salinity and temperature distributions in shallow coastal waters resulting from effluent discharge from an existing desalination plant situated on the Arabian Gulf. Parametric studies of the effects of a number of influential conditions are also carried out.

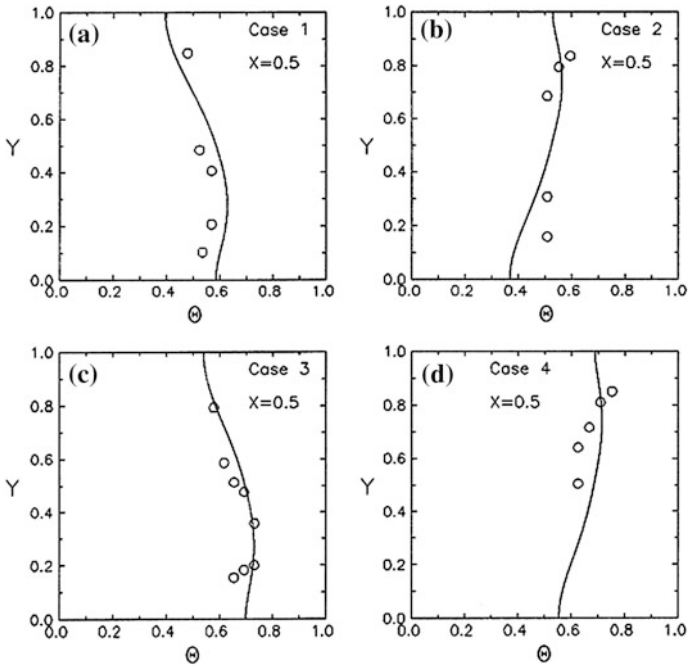

Fig. 20.3 Dimensionless temperature profiles at middle of pond (X = 0.5) for Cases 1 through 4 showing comparison between present numerical predictions (*lines*) and measurements (*circles*, Cerco 1977)

20.4.1 Seabed topography, computational domain, and parameters varied

The seabed topography of the coastal region in the vicinity of the desalination/power plant considered in the present investigation is depicted in Fig. 20.4. The depth contours are shown with values of depth given relative to a datum level which is 3 m above the mean water level. It is noted that very close to the coast, the depth contours are nearly parallel to the shoreline. This indicates that the water depth increases nearly linearly with distance away from the coastline. The first contour shown closest to the shoreline is the contour with a water depth of 6 m, relative to the datum used, and is about 50–100 m away from the shoreline. In general and as shown, the water depth increases from about 6 to 10 m, relative to the datum, in the next 100–200 m distance away from the shoreline. A large coastal region of nearly uniform water depth then persists till a distance of about 1000–1500 m away from the shoreline with a water depth of about 10–11 m, relative to the datum. This region is characterized by a coarse concentration of contour lines where the distance between consecutive contour lines is relatively wider. Beyond this region, the water depth increases continuously to over 20 m, relative to the datum, as seen at the bottom right of Fig. 20.4. Also, a reef can be noticed near the bottom left of the

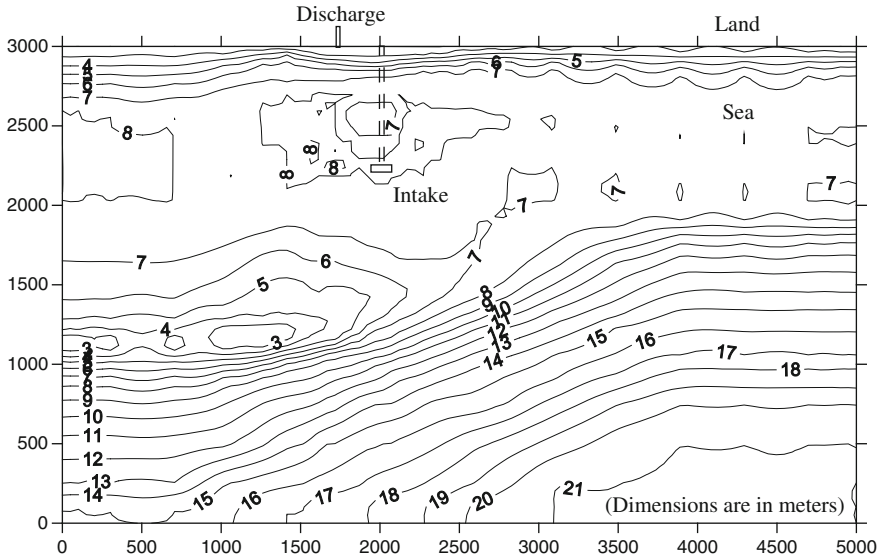

Fig. 20.4 Seabed topography in the vicinity of the desalination/power plant with water depth contour values relative to a datum level which is 3 m above the mean water level

figure where there is a concentration of contours in which the water depth gets relatively much shallower with a value of less than 5 m, relative to the datum used.

The above description of the seabed topography is accounted for in the computer model by feeding in the local values of the water depth into the finite-volume equations. As mentioned before, the local depth of flow (h) is introduced into the depth-integrated governing conservation differential equations and into their finite-volume counterparts by modifying the finite-volume areas and volume of every nodal point in the grid.

Figure 20.5 shows the calculation domain selected to encompass the coastal region in the vicinity of the plant with the dimensions, shown not to scale, extending over 5 km by 3 km along the shoreline and offshore, respectively.

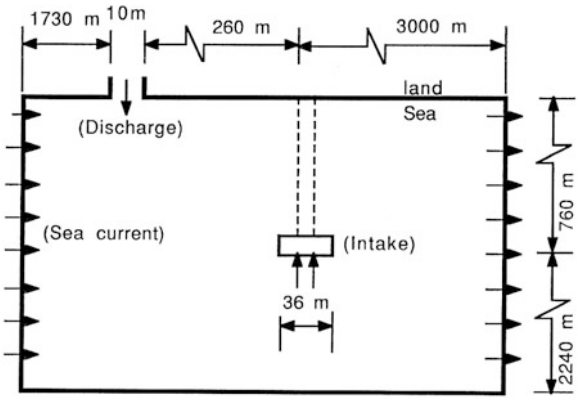

Fig. 20.5 Computational domain encompassing coastal region in vicinity of the desalination/power plant showing discharge and intake port locations and dimensions (not to scale)

Parametric studies of the effects of a number of influential conditions were carried out in order to investigate the dispersion of the heated and concentrated brine discharged into the coastal waters. This was done by using the actual seabed topography and the plant discharge and intake port locations. The parametric studies involve investigating the effects of varying: (i) sea current magnitude and direction, (ii) wind speed magnitude and direction, (iii) seawater depth in vicinity of plant, and (iv) plant discharge flow rate. Only results on the effect of sea current magnitude and direction and plant discharge flow rate are considered in the present study.

For a produced desalinated water rate of 3 m^3/s, the nominal value of the discharged mass flow rate is 55 m^3/s. In other words, 58 m^3/s of seawater, representing the feed water and the cooling water amounts, is withdrawn from the sea through the intake port, 3 m^3/s is the rate of fresh water produced, while 55 m^3/s of heated water with a higher salinity is discharged to the sea through the exit port of the plant.

The nominal values of the parameters used are summarized in Table 20.3 along with their ranges.

Detailed contours are presented, with dimensionless values of salinity and temperature in excess of nominal (ambient) seawater values, in order to determine the extent of coastal area affected by the discharged effluent. The dimensionless salinity (C) and dimensionless temperature (θ) are defined as follows:

$$C = \frac{c - c_{sea}}{c_{dis} - c_{sea}} \quad \text{and} \quad \theta = \frac{T - T_{sea}}{T_{dis} - T_{sea}} \tag{20.8}$$

where c_{sea} and T_{sea} are the nominal values far away from the discharge and intake port locations and c_{dis} and T_{dis} are, respectively, the concentration and temperature of the effluent water as discharged from the plant.

The value of c_{sea} is the nominal value of seawater salinity which is taken equal to 0.05. The value of c_{dis} is set as:

$$c_{dis} = c_{sea} + 0.01 \tag{20.9}$$

Table 20.3 The parameters varied, their nominal values and ranges

Parameter	u_{sea} (m/s)	v_{sea} (m/s)	u_{wind} (m/s)	v_{wind} (m/s)	Relative mean water level (m)	Plant desalting capacity[a] (%)
Nominal value	0.2	0.0	0.0	0.0	0.0	100
Range	0.05–0.35	−0.05–0.01	−10–2	−10–2	−1–1	75–250

[a]Plant desalting capacity relative to nominal capacity

The value of T_{sea} is set equal to the seawater equilibrium temperature (T_{eq}). The value of T_{dis} is set as:

$$T_{dis} = T_{sea} + 10 \tag{20.10}$$

It is noted that the dimensionless values of salinity (C) and temperature (θ) according to Eq. (20.8) range from 0 to 1. The value of zero corresponds to the ambient seawater value and the value of one corresponds to the value at the discharge port.

The seawater equilibrium temperature (T_{eq}) is calculated separately and independently of the plant discharge conditions. Being affected by environmental conditions, it is determined iteratively by the same computer model in the absence of interaction with the discharge and intake ports of the plant. In the present calculations, T_{eq} is calculated under the following conditions: ambient air temperature (T_{air}) of 20 °C, relative humidity (ϕ) of 60 %, and a daily-averaged solar flux absorbed of 250 W/m^2. A seawater equilibrium temperature (T_{eq}) equals to 20.9 °C is obtained and used in the simulations (Al-Sanea and Orfi 2013).

20.4.2 *Effect of Sea Current Velocity-Component Parallel to Shoreline*

The sea current is a vector quantity that has both direction and magnitude. The sea current velocity is analyzed into two components; one component is parallel to the shoreline the magnitude of which is investigated in the present section, while the other component is normal to the shoreline the magnitude of which is investigated in the next section.

The sea current velocity is one of the most important parameters expected to influence the dispersion process of the heated saline discharge in shallow coastal waters. Therefore, the salinity and temperature distributions are expected to be affected largely by the sea current velocity for two main reasons. The first reason is that the sea current determines the amount (rate) of seawater available for mixing with that amount (rate) of the discharged effluent and hence affects the dilution process. The second reason is that the sea current direction and magnitude can have determinant effect on the direction of movement of the effluent as it discharges into the sea. Certain conditions can also lead to discharge-intake port interaction causing an adverse impact on the plant operation. As mentioned above, the effect of sea current velocity component parallel to shoreline is investigated first. This is done while the sea current velocity component normal to shoreline is kept at its nominal value of zero. All other parameters are also kept at their nominal values (summarized in Table 20.3).

The sea current velocity component parallel to shoreline is varied in the range $0.05 \leq u_{sea} \leq 0.35$ m/s with an increment of 0.05 m/s. With reference to Fig. 20.4,

this direction is from left to right (i.e. from southwest direction to north east direction, which is parallel to the coastline). This is the worst case scenario under these conditions since the intake to the plant is situated at location downstream relative of the discharge from the plant. Therefore, discharge-intake interaction could be possible. Representative salinity contours with dimensionless values are shown in Fig. 20.6, for u_{sea} = 0.1, 0.15, and 0.2 m/s, respectively. These values are chosen, with u_{sea} = 0.2 m/s as the characteristic value. As will be shown, these are the most interesting among the other values over the range that u_{sea} is varied (see Table 20.3). Contour values are selected to have common presence in all figures in

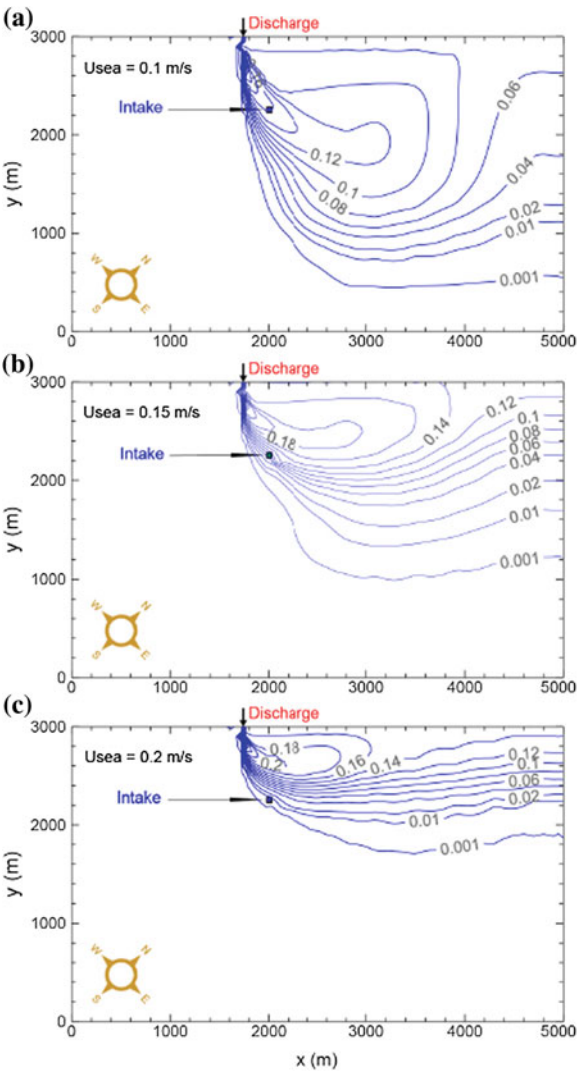

Fig. 20.6 Dimensionless salinity contours showing effect of sea current velocity component parallel to shoreline (u_{sea}); **a** u_{sea} = 0.1 m/s, **b** u_{sea} = 0.15 m/s, **c** u_{sea} = 0.2 m/s

order to facilitate comparisons and ease of interpretation. In general, the following dimensionless contour values are selected: 0.001, 0.01, 0.02, 0.04, 0.06, 0.08, 0.1, etc. generally with an interval of 0.02. The first contour value of 0.001 is considered to have effectively the ambient seawater concentration, i.e. salinities along this contour are considered to be practically unaffected by the discharge from the plant.

With reference to Fig. 20.6a where u_{sea} = 0.1 m/s, it can be seen that the sea current along the shoreline deflects the effluent discharging from the exit port of the plant in the downstream direction. Accordingly, the region far away from the coastline and the upstream region have salinities equal to the ambient sea salinity. The predictions show that the salinity increases nearer to the discharge port. Of course, at the discharge port salinity is equal to the discharge salinity from the plant having a dimensionless value of 1. The salinity at the plant intake is perhaps the most important salinity value. This location, indicated on the figure, appears to be strongly affected by the discharge conditions. The contours reveal a relative salinity at intake of about 0.16. This value results from the center of the discharged effluent passing directly over the intake under these conditions.

As u_{sea} increases to 0.15 m/s, the stronger current deflects the effluent toward the coastline, as shown in Fig. 20.6b. The contour lines compress and the coastal area affected by the discharge shrinks. However, although the affected coastline area decreases, higher salinity occurs in the region nearer to the coastline. Nevertheless, the plant intake port lies outside of the core of the plume and now has a relative salinity of 0.08, in contrast to the results shown in Fig. 20.6a. Increasing u_{sea} to 0.2 m/s, shown in Fig. 20.6c, collapses the discharged effluent onto the coast where salinity contours becoming parallel with the coastline at far downstream locations. The effluent area is now smaller, but the salinity is higher closer to coastline. Under these conditions, the intake port experiences very little of the discharged effluent. The discharged effluent lies away from the intake port, closer to the coastline, and the relative salinity near the intake port is less than 0.01.

The corresponding results for the effect of sea current velocity component parallel to shoreline on the temperature distributions are presented in Fig. 20.7. The striking feature is that the trends of variation of these contours are very similar to those of the salinity contours shown earlier in Fig. 20.6. However, by closer examination of the results, it becomes clear that there are slight differences in the absolute values of the contours. For a given location, the dimensionless temperature is slightly less than the corresponding dimensionless salinity. As a consequence, the area enclosed by a certain value of dimensionless temperature is slightly smaller than that enclosed by the same value of dimensionless salinity. This small difference between the temperature and salinity results can be attributed to the effect of heat transfer at the sea surface. By comparing the energy and concentration conservation equations (Eqs. 20.5 and 20.6, respectively) and by imposing similar boundary conditions, one might expect such an outcome by casting the results in a dimensionless form.

The close values between the dimensionless temperature and salinity, with temperature values being slightly smaller, indicate that there is a net heat loss at the water-air interface, as to be expected. However, as it turned out to be, this thermal loss is less effective, compared to the process of mixing (dispersion) between the

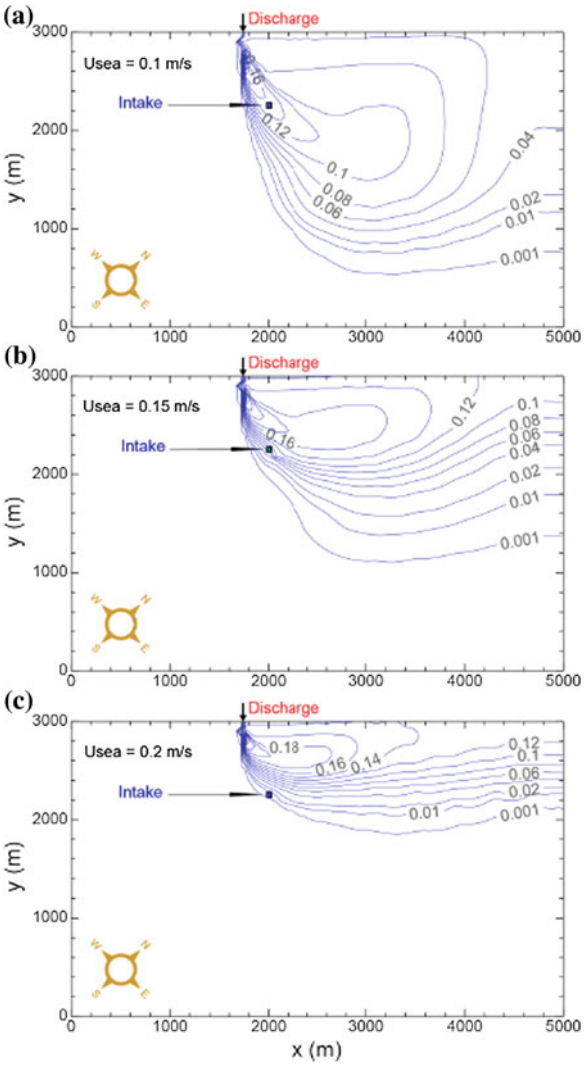

Fig. 20.7 Dimensionless temperature contours showing effect of sea current velocity component parallel to shoreline (u_{sea}); **a** u_{sea} = 0.1 m/s, **b** u_{sea} = 0.15 m/s, **c** u_{sea} = 0.2 m/s

heated discharged effluent and the cooler receiving seawater body, in altering the discharged effluent temperature. In other words, the discharged heated effluent has been cooled down dominantly by mixing with the cooler seawater than by the net heat loss from the surface under the present conditions. With regard to the salinity of the discharged effluent, this has been reduced solely by mixing with the seawater that is less saline. By suppressing the sources and sinks of heat at the water-air interface, the dimensionless temperature results should have been identical to the dimensionless salinity results.

Figure 20.8 shows the variations of the dimensionless salinity and temperature at plant intake (C_{in} and θ_{in}, respectively) with the sea current velocity-component

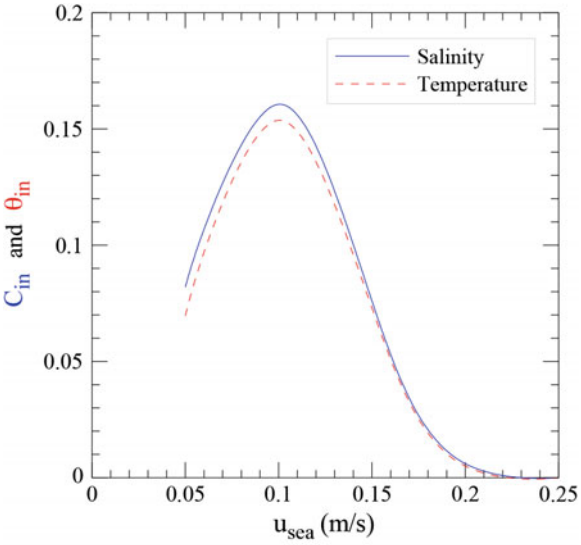

Fig. 20.8 Dimensionless salinity and temperature at plant intake port versus sea current velocity component parallel to shoreline

parallel to shoreline (u_{sea}). All other parameters are kept constant at their nominal values. The results show that the worst conditions take place at u_{sea} = 0.1 m/s at which C_{in} and θ_{in} assume their highest values as far as this parameter is concerned. Under such conditions, the location of the intake port of the plant coincides with the center of the effluent expelled from the plant discharge port. At values of u_{sea} smaller or higher than u_{sea} = 0.1 m/s, the intake port falls on the edges of the discharged effluent. At u_{sea} > 0.2 m/s, the intake port almost completely escapes the influence of the effluent. The contour plots shown previously in Figs. 20.6 and 20.7, for salinity and temperature, respectively, help clarify and further explain the present results. It is interesting to note that, for a given u_{sea}, values of the dimensionless temperature are always smaller than values of dimensionless salinity. This relative reduction in temperature is attributed to net heat loss from the water surface due to temperatures elevated above the equilibrium temperature.

Table 20.4 summarizes values of dimensionless and dimensional salinity (C_{in} and c_{in}) as well as dimensionless and dimensional temperature (θ_{in} and T_{in}) at plant intake

Table 20.4 Dimensionless and dimensional salinities (C_{in} and c_{in}) and temperatures (θ_{in} and T_{in}) at plant intake for different sea current velocity-component parallel to shoreline (u_{sea})

	u_{sea} (m/s)						
	0.05	0.1	0.15	**(0.2)**	0.25	0.3	0.35
C_{in} × 100	8.197	16.06	7.6	0.6034	0.0	0.0	0.0
c_{in} × 100	5.082	5.161	5.076	5.006	5.000	5.000	5.000
θ_{in} × 100	6.954	15.37	7.299	0.5003	0.0	0.0	0.0
T_{in} (°C)	21.60	22.44	21.63	20.95	20.90	20.90	20.90

for different sea current velocity-component parallel to shoreline (u_{sea}). All other parameters are kept constant at their nominal values. The number in parenthesis and bold in the table is the nominal value of the parameter under consideration.

20.4.3 *Effect of Sea Current Velocity-Component Normal to Shoreline*

The effect of sea current velocity-component normal to shoreline (v_{sea}) is investigated while keeping the parallel component constant at the nominal value of $u_{sea} = 0.2$ m/s. All other parameters are kept at their nominal (representative) values. The values of v_{sea} investigated are:−0.05, −0.04, −0.03, −0.02, −0.01, 0.0, and 0.01 m/s. The negative value is in the direction away from the shoreline, the positive value is toward the shoreline, while the zero is the nominal value of this parameter. Representative salinity contours are presented in Fig. 20.9 for $v_{sea} = -0.04$, −0.02, and 0.01 m/s, respectively.

As clearly seen from Fig. 20.9a, with $v_{sea} = -0.04$ m/s, away from shoreline, the effluent spreads far into the sea covering a relatively large area. As a result, the intake port is significantly affected with the relative salinity at the intake of about 0.08. As v_{sea} is decreased to −0.02 m/s (Fig. 20.9b) the seaward effluent spread is reduced and the affected area becomes smaller. However, this takes place at the expense of increasing salinity close to the shoreline. The salinity at the intake port is reduced now to about 0.04 (half of the previous value) as a result of a relatively larger effluent deflection toward the shoreline. This salinity at the intake port is further reduced to about 0.001 as shown in Fig. 20.9c, for $v_{sea} = 0.01$ m/s. Under the present conditions, sea current velocity component toward the shoreline acts to reduce the effluent spread. The area of spread is now much smaller and is confined closer to the shoreline but with, of course, much higher salinity concentration. An intermediate stage between the results in Fig. 20.9b and c is that for $v_{sea} = 0.0$ with results already presented in Fig. 20.6c. Plots and tabulated values of salinity at plant intake as affected by v_{sea} are presented later.

The corresponding temperature distributions are presented in Fig. 20.10 showing the effect of v_{sea}. As mentioned earlier, these distributions resemble those of the salinity distributions but with dimensionless values that are slightly smaller.

Figure 20.11 shows the dependence of the dimensionless salinity and temperature at plant intake (C_{in} and θ_{in}, respectively) on the sea current velocity-component normal to shoreline (v_{sea}). Of course, all other parameters are kept constant at their nominal values including the resetting of u_{sea} to its nominal value of $u_{sea} = 0.2$ m/s. The −ve values of v_{sea} designate the direction away from the shoreline; such a direction for v_{sea} increases the possibility of discharge-intake port interaction. Indeed, the results show that C_{in} and θ_{in} increase with increasing v_{sea}, in this negative direction, as the intake port location becomes closer to the center of the discharged effluent. On the other side, as $v_{sea} = 0$ (the default value) or becomes

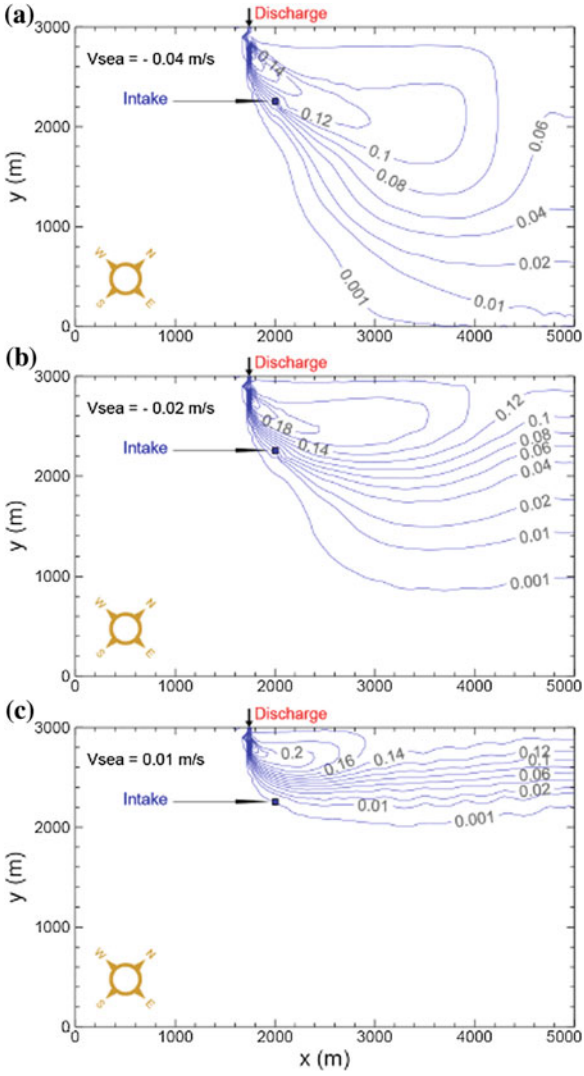

Fig. 20.9 Dimensionless salinity contours showing effect of sea current velocity component normal to shoreline (v_{sea}); **a** $v_{sea} = -0.04$ m/s, **b** $v_{sea} = -0.02$ m/s, **c** $v_{sea} = 0.01$ m/s (−ve is away from shoreline and +ve is toward shoreline)

+ve, the values of C_{in} and θ_{in} become extremely small indicating practically no discharge influence on the intake conditions.

Table 20.5 summarizes values of dimensionless and dimensional salinity (C_{in} and c_{in}) as well as dimensionless and dimensional temperature (θ_{in} and T_{in}) at plant intake for different sea current velocity-component normal to shoreline (v_{sea}). The value written in parenthesis and bold in the table is the nominal value of the parameter under consideration.

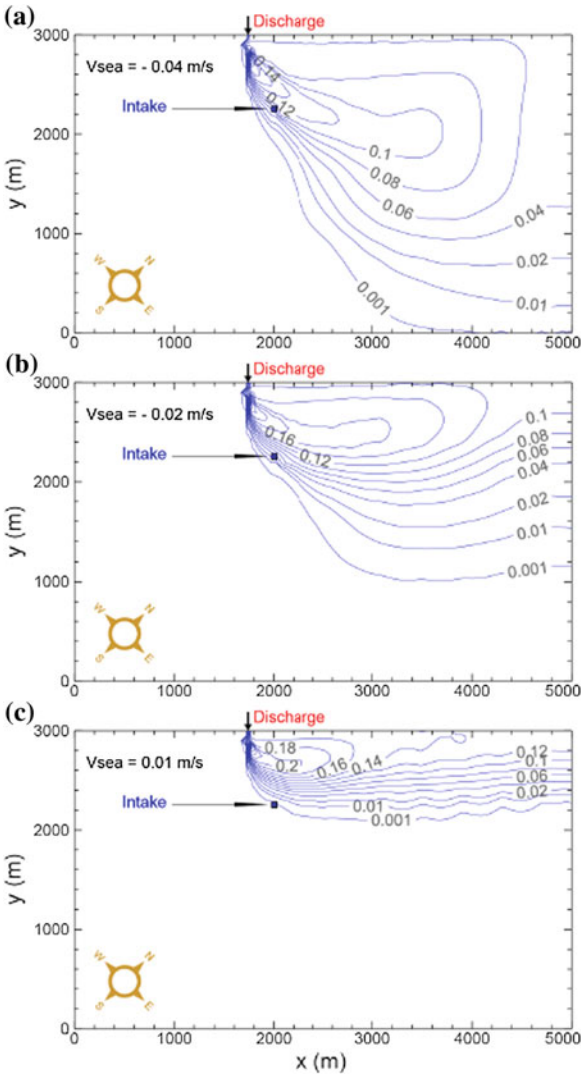

Fig. 20.10 Dimensionless temperature contours showing effect of sea current velocity component normal to shoreline (v_{sea}); **a** $v_{sea} = -0.04$ m/s, **b** $v_{sea} = -0.02$ m/s, **c** $v_{sea} = 0.01$ m/s (−ve is away from shoreline and +ve is toward shoreline)

20.4.4 Effect of Plant Desalting Capacity

The effect of varying mass flow rate of the effluent discharged from the exit port of the power/desalination plant is presented and analyzed in this section. This mass flow rate is taken to be proportional to the desalting capacity of the plant. The nominal value of the discharged mass flow rate, for a 3000 kg/s of produced desalinated water, is 55,000 kg/s.

The scenario of investigating the effect of varying plant desalting capacity is not really hypothetical since it involves possible upgrading of the current existing plant,

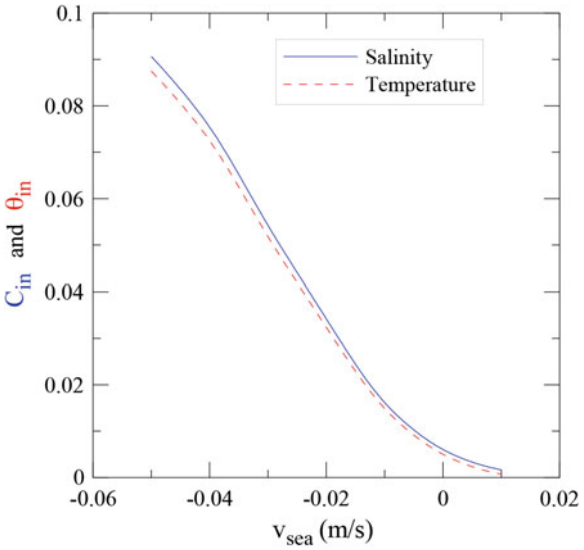

Fig. 20.11 Dimensionless salinity and temperature at plant intake port versus sea current velocity component normal to shoreline (−ve v_{sea} is in direction away from shoreline and +ve is toward shoreline)

Table 20.5 Dimensionless and dimensional salinities (C_{in} and c_{in}) and temperatures (θ_{in} and T_{in}) at plant intake for different sea current velocity-component normal to shoreline (v_{sea})

	v_{sea} (m/s)						
	−0.05	−0.04	−0.03	−0.02	−0.01	**(0.0)**	0.01
$C_{in} \times 100$	9.062	7.539	5.422	3.421	1.616	0.6034	0.1652
$c_{in} \times 100$	5.091	5.075	5.054	5.034	5.016	5.006	5.002
$\theta_{in} \times 100$	8.748	7.249	5.180	3.238	1.488	0.5003	0.0712
T_{in} (°C)	21.77	21.62	21.42	21.22	21.05	20.95	20.91

building a new plant, or working with less than full plant capacity. Therefore, the following percentages of plant desalting capacity are considered relative to the nominal capacity: 75, 100 % (the nominal case), 125, 150, 200, and 250 %. For this study, the intake and discharge flow rates were proportionally altered.

Representative temperature contours are shown in Fig. 20.12, for plant desalting capacity of 75, 125, and 200 %, respectively, with the nominal results already presented in Fig. 20.6c. The results show that with increasing plant discharge flow rate, the effluent spreads further into the sea covering a wider area. In doing so, the temperature increases in the region far away from the shoreline and decreases in the region close to the shoreline. This is attributed to increasing amount of hot discharge and increasing momentum of the issuing effluent with increasing plant desalting capacity. The increase in momentum, results in smaller deflection of effluent by the sea current and hence smaller temperature gradients in the region close to the shoreline. As seen, the intake port gets exposed to the discharged effluent with increasing plant desalting capacity. While the intake port almost

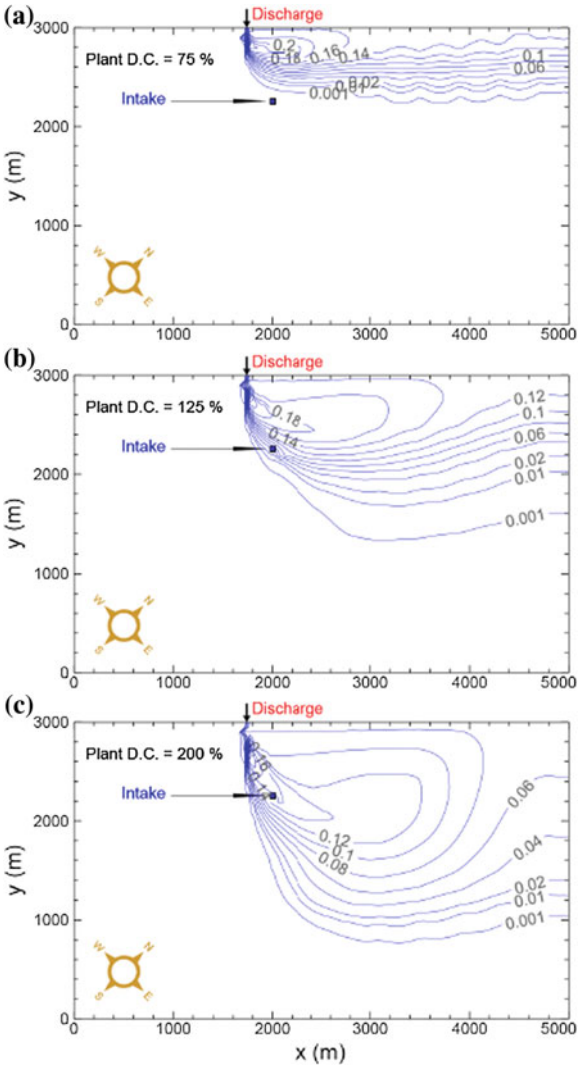

Fig. 20.12 Dimensionless temperature contours showing effect of plant desalting capacity (PDC) as a percentage of nominal capacity; **a** PDC = 75 %, **b** PDC = 125 %, **c** PDC = 200 %

completely experiences little influence from the discharge plume under the conditions in Fig. 20.12a, in Fig. 20.12c it lies directly in the path of the core of the plume under the conditions shown in Fig. 20.12c. The corresponding salinity contours, not presented here, show similar distributions to the isotherms.

Table 20.6 summarizes values of dimensional salinity (c_{in}) as well as dimensional temperature (T_{in}) at plant intake for different plant desalting capacities relative to nominal capacity. The plant desalting capacity is measured as a percentage of the plant nominal capacity (the nominal capacity being 100 %). All other parameters are kept constant at their nominal values. The value written in parenthesis and bold in

Table 20.6 Dimensional salinity (c_{in}) and temperature (T_{in}) at plant intake for different plant desalting capacities relative to nominal capacity

	Plant desalting capacity relative to nominal capacity (%)					
	75	**(100)**	125	150	200	250
$c_{in} \times 100$	5.000	5.006	5.049	5.103	5.159	5.162
T_{in} (°C)	20.9	20.95	21.37	21.90	22.45	22.47

Table 20.6 is the nominal value for the plant desalting capacity. As shown, salinity and temperature at the intake were nearly unaffected by the discharge for a plant desalting capacity <100 %, i.e. there is no noticeable discharge-intake port interaction. However, c_{in} and T_{in} increased continuously with increasing plant capacity and reached their highest values (the worst conditions) at a plant capacity of about 200 %. At the latter value, the center of the discharged effluent passes through the intake port. The contour plots for temperature shown previously in Fig. 20.12 give further clarification of the present results.

20.5 Conclusions

The present chapter presented and discussed results obtained from a numerical model for the dispersion of concentrated, heated brine in a shallow coastal region. The mathematical model was based on the shallow-water approximations in which the governing equations were depth averaged by assuming negligible variations of velocity, temperature, and salinity over the depth and by neglecting the vertical velocity component, thus rendering the problem to be two-dimensional. Appropriate boundary conditions were used.

The application was made for a desalination/power plant situated on the Arabian Gulf in KSA. The seabed topography of the coastal area in the vicinity of the plant was used in the study.

Parametric studies evaluated the effects of varying sea current magnitude and direction and plant discharge flow rates. The results were presented, for generalization, in the form of dimensionless salinity (C) and dimensionless temperature (θ). This was done by normalizing the salinity (c) and temperature (T) by reference values for the nominal seawater far away from the plant (c_{sea} and T_{sea}) and by reference values for nominal salinity and temperature at the plant discharge port (c_{dis} and T_{dis}). Contours were presented, with values of salinity and temperature in excess of nominal seawater values, which could be used to determine the extent of coastal area affected by the discharged effluent.

Possible plant discharge-intake port interactions were predicted with varying degrees of strength depending upon the various conditions. The results presented indicate such interactions and quantified values of salinity and temperature at the plant intake port (C_{in} and θ_{in}) for different scenarios. For a given set of conditions,

salinity contour shapes were shown to be very similar to those of temperature, and dimensionless salinity and temperature values were predicted to be close to each other. This indicated that the heat and mass transfer analogy was approximately valid under the present conditions. For the range of parameters considered, the following results could be summarized:

- C_{in} and θ_{in} increased from 0 (negligible discharge-intake port interaction) to 0.16 as a result of varying sea current magnitude and direction.
- C_{in} and θ_{in} increased from 0 to 0.16 as a result of increasing plant discharge flow rate.

The above values of C_{in} and θ_{in} in excess of zero, which took place under certain conditions, indicated discharge-intake port interaction, in which the plant would withdraw seawater with salinity and temperature higher than the nominal seawater values. As a result, plant thermal efficiency would decrease and energy required for desalination increase. Possible remedies include increasing distance between intake and discharge ports and/or constructing artificial partitions, to reduce short-circuiting, both of which could require substantial capital cost.

Acknowledgments This project was supported by NSTIP strategic technologies program number (08-ENV405-2) in the Kingdom of Saudi Arabia.

References

Abdul Azis, P. K., Al-Tisan, I., Al-Daili, M., Green, T. N., Ghani, A., Dalvi, I., & Javeed, M. A. (2000). Effects of environment on source water for desalination plants on the eastern coast of Saudi Arabia. *Desalination, 132*, 29–40.

Abou-Elhaggag, M. E., El-Gamal, M. H., & Farouk, M. I. (2011). Experimental and numerical investigation of desalination plant outfalls in limited disposal areas. *Journal of Environmental Protection, 2*, 828–839.

Ahmed, M., Shayya, W. H., Hoey, D., Mahendran, A., Morris, R., & Al-Handaly, J. (2000). Use of evaporation ponds for brine disposal in desalination plants. *Desalination, 130*, 155–168.

Alameddine, I., & El-Fadel, M. (2007). Brine discharge from desalination plants: A modelling approach to an optimized outfall design. *Desalination, 214*, 241–260.

Al-Barwani, H. H., & Purnama, A. (2007). Re-assessing the impact of desalination plants brine discharges on eroding beaches. *Desalination, 204*, 94–101.

Al Mutaz, I. (1991). Environmental impact of seawater desalination plants. *Environmental Monitoring and Assessment, 16*, 75–84.

Al-Sanea, S. A., Pun, W. M., & Spalding, D. B. (1980). Computation of two-dimensional elliptic flows, including heat transfer. In K. Morgan, C. Taylor, & C. A. Brebbia (Eds.), *Computer Methods in Fluids* (pp. 217–256). London: Pentech Press.

Al-Sanea, S. A. (1982). *Numerical modeling of two-dimensional shallow-water flows*. Ph.D. thesis, Department of Mechanical Engineering, Imperial College of Science and Technology, London, UK.

Al-Sanea, S. A. (1993). Computation of the flow and salinity distribution in the vicinity of discharge and intake ports of a desalination plant. Journal of King Saud University, *5*, Engineering Science, *1*, 123–140.

Al-Sanea, S. A. (2010). Computational fluid dynamics applied to free-surface flows. Lecture 4 in Course ME 596: Selected Topics in Thermo-fluids (Part 1), Department of Mechanical Engineering, King Saud University, Riyadh.

Al-Sanea, S., & Orfi, J. (2013). Environmental impact and solutions for desalination plant discharge into shallow coastal regions (215 p). Final Report, NPST-KSU, Project: 08-ENV405–2, Riyadh, KSA.

AlZahrani, A. (2013). *Energy and exergy analysis of desalination and dual purpose plants*. MSC thesis, Department of mechanical engineering, King Saud University, KSA.

Bleninger, T. (2006). Coupled 3D hydrodynamic models for submarine outfalls. In *Environmental Hydraulic Design and Control of Multiport Diffusers.* Germany: University of Karlsruhe.

Bleninger, T., & Jirka, G. H. (2010). Environmental planning, prediction and management of brine discharges from desalination plants (237 p). Final report, Middle East Desalination Research Center, MEDRC Project: 07-AS-003, Muscat, Oman.

Cerco, C. F. (1977). *Experimental and analytical study of the design of shallow cooling ponds*. MS thesis, Department of Civil Engineering, MIT, Cambridge, Massachusetts.

Cipollina, A., Bonfiglio, A., Micale, G., & Brucato, A. (2004). Dense jet modelling applied to the design of dense effluent diffusers. *Desalination, 167*, 459–468.

Danoun, R. (2007). Desalination plants: Potential impacts of brine discharge on marine life (55 p). Final Project Report, University of Sydney.

Doneker, R. L., & Jirka, G. H. (2001). CORMIX-GI systems for mixing zone analysis of brine wastewater disposal. *Desalination, 139*(1–3), 263–274. doi:10.1016/S0011-9164(01)00318-6.

Fernadez, A. L., Ferrero-Vicente, L. M., Marco-Mendez, C., Martinez- Garcia, E., Zubcoff, J., & Sanchez-Lizaso, J. L. (2012). Comparing four mixing zone models with brine discharge measurements from a reverse osmosis desalination plant in Spain. *Desalination, 286*, 217–224.

Hoepner, T. (1999). A procedure for environmental impact assessments (EIA) for seawater desalination plants. *Desalination, 124*, 1–12.

Kuipers, J, & Vreugdenhil, C. B. (1973). Calculations of two-dimensional horizontal flow. Report S 163, Part I, Delft Hydraulics Lab, Netherlands.

Lattemann, S. (2009). Protecting the marine environment. In A. Cipollina, G. Micale, & L. Rizzuti (Eds.), *Sea Water Desalination* (pp. 273–299). Berlin: Springer.

Lattemann, S., Kennedy, M., Schippers, J., & Amy, G. (2009). Global desalination situation. In I. Escobar & A. Schäfer (Eds.), *Sustainable Water for the Future* (pp. 7–39). The Netherlands: Elsevier.

Malcangio, D., & Petrillo, A. F. (2010). Modeling of brine outfall at the planning stage of desalination plants. *Desalination, 254*, 114–125.

Munoz, I., & Fernandez-Alba, A. R. (2008). Reducing the environmental impacts of reverse osmosis desalination by using brackish groundwater resources. *Water Research, 42*, 801–811.

Oliver, C. J., Davidson, M. J., & Nokes, R. I. (2013). Predicting the near field of desalination discharges in a stationary environment. *Desalination, 309*, 148–155.

Palomar, P., & Losada, I. (2011). Impacts of brine discharge on the marine environment. modelling as a predictive tool, Chapter 3. In: *Desalination, Trends and Technologies* (pp. 279–310) www.intechopen.com.

Palomar, P., Lara, J. L., & Losada, I. J. (2012a). Near field brine discharge modeling part 2: Validation of commercial tools. *Desalination, 290*, 28–42.

Palomar, P., Lara, J. L., Losada, I. J., Rodrigo, M., & Alvárez, A. (2012b). Near field brine discharge modeling part 1: Analysis of commercial tools. *Desalination, 290*, 14–27.

Patankar, S. V., & Spalding, D. B. (1972). A calculation procedure for heat, mass and momentum transfer in three-dimensional parabolic flows. *International Journal of Heat and Mass Transfer, 15*, 1787–1806.

Patankar, S. V. (1980). *Numerical Heat Transfer and Fluid Flow*. Washington, DC: Hemisphere Publishing Corporation.

Pun, W. M., & Spalding, D. B. (1977). *A general computer program for two-dimensional elliptic flows*. Report no. HTS/76/2, Department of Mechanical Engineering, Imperial College of Science and Technology, London, UK.

Purnama, A., Al-Barwani, H. H., & Al-Lawatia, M. (2003). Modeling dispersion of brine waste discharges from a coastal desalination plant. *Desalination, 155*, 41–47.

Purnama, A., & Al-Barwani, A. A. (2005). Some criteria to minimize the impact of brine discharge into the sea. *Desalination, 171*, 167–172.

Purnama, A., & Al-Barwani, H. H. (2006). Spreading of brine waste discharges into the Gulf of Oman. *Desalination, 195*, 26–31.

Rodi, W. (1978). *Turbulence models and their application in hydraulics—a state of the art review*. Report no. SFB 80/T/127, University of Karlsruhe, Germany.

Shao, D. D., Law, A. W. K., & Li, H. Y. (2008). Brine discharges into shallow coastal waters with mean and oscillatory tidal currents. *Journal of Hydro-environment Research, 2*, 91–97.

Sharqawy, M. H., Lienhard V, J. H., & Zubair, S. M. (2011). On exergy calculations of seawater with applications in desalination systems. *International Journal of Thermal Sciences, 50*, 187–196.

Spalding, D. B. (1975). Transfer of heat in rivers, bays, lakes and estuaries. THIRBLE, Report No. HTS/75/4, Department of Mechanical Engineering, Imperial College of Science and Technology, London, UK.

Zhao, D., Xue, J., Li, S., Sun, H., & Zhang, D. Q. (2011). Theoretical analyses of thermal and economical aspects of multi-effect distillation desalination dealing with high-salinity wastewater. *Desalination, 273*, 292–298.